Tim Sluiter

The interaction of a submerged floating tunnel with a moving vehicle

The interaction of a submerged floating tunnel with a moving vehicle.

By

Tim Sluiter
4540883

In partial fulfilment of the requirements for the degree of

Bachelor of Science
in Civil Engineering

at the Delft University of Technology,

Supervisor: K.N. van Dalen
A. Faragau

18 June 2019

TU Delft

Preface

To fulfill the requirements of the bachelor's in civil engineering at TU Delft, this bachelor thesis is the final assignment. The choice of subject for this thesis was triggered during the second-year course CTB2300 – DYNAMICS OF SYSTEMS. All the dynamics courses have interested me since year one, as well as the Hydraulic Engineering courses. To be able to do dynamic study on the Submerged Floating Tunnel, both of my interests were being fulfilled. Therefore, I would like to thank Professor K.N. van Dalen for this opportunity and being my first supervisor.

Furthermore, I would like to thank my second supervisor A. Faragau. Both have always been very helpful and supportive during the whole process of this thesis. The lessons learned during this dissertation, especially during the struggles of the coding and the difficulties during the analyses will be remembered and will be very helpful in the future.

Tim Sluiter, Delft, 18 June 2019

Summary

Due to the high cost of long spanned bridges or deep tunnels, the interest into a submerged floating tunnel (SFT) has reemerged. In the last twenty years many studies on the SFT have been performed. This report investigates the interaction between a single vehicle, moving at constant velocity, and the SFT. The research is limited to the dynamic response, of both vehicle and tunnel, in only the vertical direction. The SFT is moored to the bed floor and is further kept in position by the buoyance force.

The main question to be answered is: Does the vehicle's inertia, the design of the SFT (i.e., the length of the tunnel) or the vehicle parameters, because of this dynamic loading, play a significant role in the Ultimate Limit State of the tunnel or the Service Limit State for passenger.

A schematization of the model is shown in Figure 1. The vehicle is schematized as a two degree of freedom system and for the tunnel the Euler-Bernoulli beam equation is used. The tether and the fluid forces are modeled as external forcing, which lead to the following set of equations:

$$M\frac{\partial^2 u(t)}{\partial t^2} = Mg - Q_1(t) - Q_2(t),$$
$$J\frac{\partial^2 \theta(t)}{\partial t^2} = -\frac{W}{2}Q_1(t) + \frac{W}{2}Q_2(t),$$
$$EI\frac{\partial^4 w(x,t)}{\partial x^4} + \rho A\frac{\partial^2 w(x,t)}{\partial t^2} = g(x,t) + F_s + F_{drag}.$$

To solve for the deflection of the tunnel, Modal expansion is applied. The system of equations is then solved numerically, using MATLAB's 'ode45'-solver. The system is validated in the limit cases against Graff's (1975) known solution for a constant load moving across a simply supported beam.

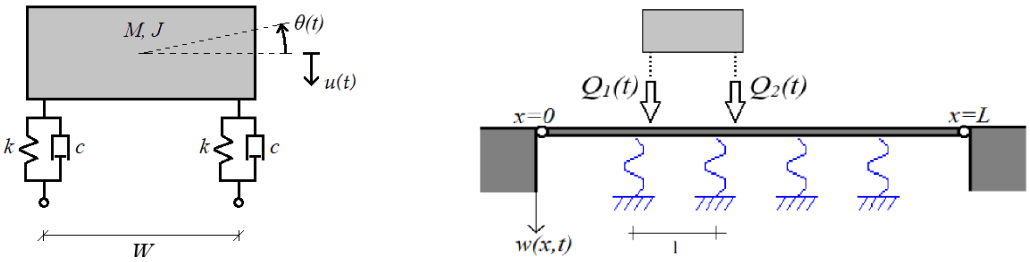

Figure 1 Left: Schematization of the vehicle. Right: Schematization of the tunnel with the interaction forces.

This research has shown that the inertia of a single vehicle plays no significant effect on the displacement of the tunnel. The movement of the loads on the other hand plays a significant effect on the behavior of the tunnel, especially around resonant velocity.

Close to resonant velocity, the length of the tunnel shows a large increase in the displacements of the tunnel and a significant increase in vertical accelerations of the vehicle. This resonant velocity did not increase for longer tunnels, which explains that the passing of the tethers at a certain velocity is the effect of this resonance. The displacements can increase more than three times compared to lower velocities. The accelerations of the vehicle do not lead to

uncomfortable conditions.

The spacing of the tethers influences the magnitude of the resonant velocities. Combined with the impact of the stiffness of the tethers investigated in 2011 (Tariverdilo, Mirzapour, Shahmardani, Shabani, & Gheyretmand), a dynamic study is always advised for the structural integrity of the tunnel. It needs further investigation if the resonant velocity might be inversely proportional to the spacing between the tethers.

The vehicle's spring stiffness and dashpot coefficient do lead to different motion patterns of the vehicle but only lead to unacceptable accelerations for a very stiff vehicle spring neglecting the dashpot.

It is suggested that more research is done to the interaction between moving vehicles and the SFT, by increasing the number of vehicles or train carts. Also, the impact of the loading in horizontal direction (i.e., the flow of the fluid) on the resonant velocity and the displacements would be interesting.

Contents

1. Introduction

To cross waterbodies, a bridge or a tunnel is often chosen. One of the disadvantages of a bridge is the deck height, which restricts the vessel size in these waterbodies. The alternative, that is mostly considered, is a tunnel underneath the water. When these waterbodies get deep and wide, such as deep lakes or fjords, it is more difficult and more expensive to realize the above two options.

A submerged floating tunnel (SFT) could be an alternative to cross wide and deep waterbodies. The first feasibility study of an SFT dates already to 1971, by the Norwegian Public Roads Administration (Remseth, Leira, Okstad, Mathisen, & Haukås, 1999). In recent years, the interest in this alternative has reemerged due to the high cost of long spanned bridges or tunneling under these deep waterbodies. Although researchers and engineers think it is a plausible option to build a submerged floating tunnel, one has yet to be build (Chow, 2019). A few of the main reasons such a tunnel has not yet been built are the uncertainties and potential risks in the building process.

Over the last twenty years many studies have been performed regarding the SFT. These studies vary from investigating specific structural elements to the dynamic response of the SFT to hydrodynamic loading. The latter has been investigated as well as seismic responses by Pilato, Perotti and Fogazzi (2008). Xiang and Yang (2017) investigated the response of the SFT to impact loading, where a single impact was induced.

Another safety concern could be the possibility of resonance due to the interaction between a moving vehicle and the SFT. Tariverdilo, Mirzapour, Shahmardani, Shabani and Gheyretmand (2011) mostly investigated the impact of the cable stiffness om the vibrations of the tunnel by a moving constant load. Research has also been done by Yang, Yau & Wu (2004) on vehicle-bridge interaction and the importance of the vehicle's inertia. Their research was limited to a simple beam and a three spanned bridge. Although, the vehicle-fluid-tunnel interaction has been investigated in 2018 (Lin, Xiang, Yang, & Chen), the importance of vehicle inertia on the SFT has not been investigated. They investigated the impact of the flow velocity, the buoyance weight ratio and the angle of the supports. They also found that the displacement and bending moments are amplified by the vehicle-tunnel interaction.

This thesis will further investigate the interaction between a single vehicle, moving at constant velocity, and a submerged floating tunnel. More specifically, if the influence of the vehicle inertia, the design of the SFT (i.e., the tether spacing) or the vehicle parameters play a significant role in the Ultimate Limit State (ULS) of the tunnel or the Service Limit State (SLS) for passenger comfort. The submerged floating tunnel in this report, is kept in position through the buoyance force and cables moored to the bed floor of a waterbody. The research is limited to the response in the vertical direction only.

This study follows earlier research done by Bilal Ouchene and Anne de Graaf, who investigated the interaction of a vehicle with a simply supported bridge. Consequently, for benchmarking the implemented solution a small investigation is also done on the influence of dynamic loading on the simply supported beam.

The structure of this thesis is as follows. In chapter 2 the theoretical model is explained. Chapter 3 presents the solution method and its validation. In chapter 4 the results will be displayed for a simply supported beam and the SFT. The conclusion and the recommendations are found in chapter 5. At last, the references are displayed, followed by the appendices.

2. The theoretical model and the solution method

In this chapter the theoretical model to represent the submerged floating tunnel and the moving vehicle is described. In paragraph 2.1 is the simplified model presented. Paragraph 2.2 gives the equations of motion for the vehicle. In 2.3 Euler-Bernoulli beam equation is used to describe the tunnel. To finish with paragraph 2.4 where the solution method is explained.

2.1 The model

The vehicle is simplified to a two degrees of freedom system which is schematized in Figure 2. The displacement of the vehicle is represented with $u(t)$, where t denotes time and the rotation around its own center of mass is represented by $\theta(t)$. The wheel axle is represented by a spring with spring constant k and a dashpot with damping coefficient c. The vehicle's mass is denoted by M and its inertia by J; also, the wheelbase is represented as W.

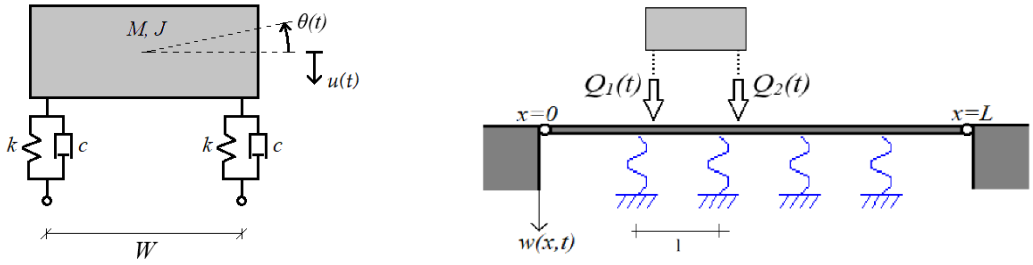

Figure 2 Left: Schematization of the vehicle (De Graaf, 2018). Right: the schematization of the tunnel and the interaction with the vehicle (De Graaf, 2018). The tethers modelled as spring supports.

The tunnel is simply supported at the boundaries and its tethers are modelled as spring supports, separated from each other with length l. The total length of the tunnel is denoted by L. The displacement of the tunnel is represented by $w(x,t)$. The vehicle travels with a constant velocity v. The contact forces between tunnel and vehicle are represented by $Q_1(t)$ and $Q_2(t)$. Also, the interaction force with the fluid is considered and denoted as F_{fluid}.

2.2 Equations of motion for the vehicle.

The behavior of the vehicle is described by the following equations of motion:

$$M\frac{\partial^2 u(t)}{\partial t^2} = Mg - Q_1(t) - Q_2(t), \tag{2.1}$$

$$J\frac{\partial^2 \theta(t)}{\partial t^2} = -\frac{W}{2}Q_1(t) + \frac{W}{2}Q_2(t), \tag{2.2}$$

where:

$$Q_1(t) = k\left[u(t) + \frac{W}{2}\theta - w(x = vt - W, t)\right] + c\left[\frac{\partial u(t)}{\partial t} + \frac{W}{2}\frac{\partial \theta}{\partial t} - \frac{\partial w(x = vt - W, t)}{\partial t}\right],$$

$$Q_2(t) = k\left[u(t) - \frac{W}{2}\theta - w(x = vt, t)\right] + c\left[\frac{\partial u(t)}{\partial t} - \frac{W}{2}\frac{\partial \theta}{\partial t} - \frac{\partial w(x = vt, t)}{\partial t}\right].$$

(2.3)

The initial conditions need to be considered. At time $t = 0$ the vehicle is assumed to be at rest. An initial displacement due to the gravity is acting on the vehicle. This leads to the following initial conditions:

$$u(0) = \frac{Mg}{2k}, \qquad \frac{\partial u}{\partial t}(0) = 0,$$

$$\theta(0) = 0, \qquad \frac{\partial \theta}{\partial t}(0) = 0.$$

(2.4)

2.3 Euler-Bernoulli beam equation

The Euler-Bernoulli beam equation is used to represent the behavior of the submerged tunnel (Spijkers, Vrouwenvelder, & Klaver, 2005):

$$EI\frac{\partial^4 w(x,t)}{\partial x^4} + \rho A\frac{\partial^2 w(x,t)}{\partial t^2} = g(x,t) + F_s + F_{fluid},$$

(2.5)

where EI represents the bending stiffness, ρA the mass per unit length, $g(x,t)$ the loads from the interaction with the vehicle and F_s the forcing from the tethers.

The displacement of the tunnel is considered relative to the displacement of the dead load. Consequently, the initial conditions are given by:

$$w(x,0) = 0, \qquad \frac{\partial w}{\partial t}(x,t) = 0.$$

The boundary conditions for the simply supported beam are given by:

$$w(0,t) = 0, \qquad \frac{\partial^2 w}{\partial t^2}(0,t) = 0,$$

$$w(L,t) = 0, \qquad \frac{\partial^2 w}{\partial t^2}(L,t) = 0.$$

Interaction Forces between vehicle and tunnel

The position of the contact forces Q_1 and Q_2 are $v * t - W$ and $v * t$, respectively. These are represented with the Dirac delta function $\delta(x - (vt - W))$ and $\delta(x - vt)$ (Q_1 is travelling a wheelbase behind Q_2). Mathematically a Heaviside function will be added, because the tunnel will only register the forces while the vehicle is in the tunnel. These Heaviside functions are:

$$H\left(t - \frac{W}{v}\right) - H\left(t - \frac{L+W}{v}\right) \; for \; Q_1,$$

and:

$$H(t) - H\left(t - \frac{L}{v}\right) for \; Q_2.$$

This leads to:

$$g(x,t) = Q_1 * \ \delta\big(x-(vt-W)\big) * \left(H\left(t-\frac{W}{v}\right) - H\left(t-\frac{L+W}{v}\right)\right) + Q_2 * \ \delta\big(x-(vt)\big) * \left(H(t) - H\left(t-\frac{L}{v}\right)\right) \tag{2.6}$$

The tether forcing

The forcing from the tethers is represented as an external load. This is chosen for mathematical reasons, which are explained later in this chapter. The tethers are placed periodically, with a distance l apart from one another. A schematization of the tunnel's design and the angles of the tethers and the corresponding forcing in the vertical direction are shown in Figure 3. The sag of the cables due to the gravitational pull effectively changes the young's modulus of the cables (Lin, Xiang, & Yang, 2016), this affect is not taken into account.

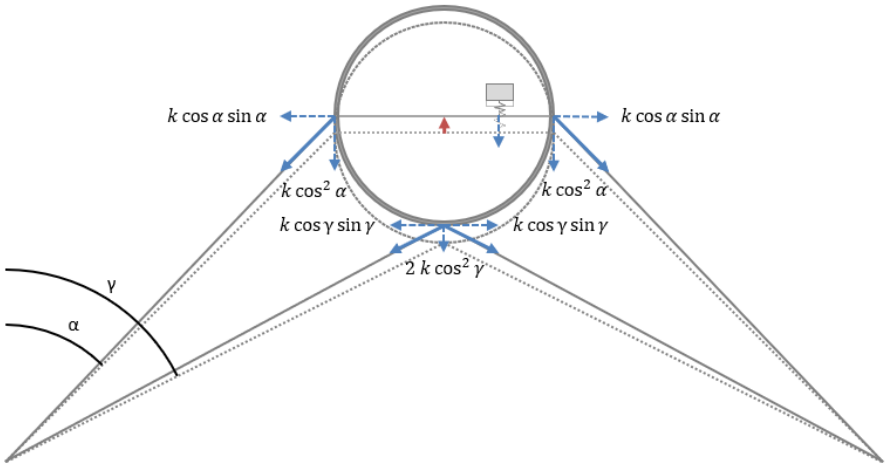

Figure 3 Cross-sectional view of the schematization of the tunnel and it's tethers with the corresponding factors to determine the forcing in vertical direction (La Zara, 2019)

This leads to the following equation describing the forcing on the tunnel in vertical direction exerted by the tethers:

$$F_s(x,t) = \sum_{p=1}^{p=\frac{L}{l}-1} k_z(2\cos^2(\alpha) + 2\cos^2(\gamma))\ w(x=pl,t)\ )\delta(x-pl), \tag{2.7}$$

where $k_z = \frac{E_c A_c}{l_{cable}}$, in which Ec represents the Young's Modulus of the tether, A_c the cross-sectional area of the cable and l_{cable} the length of the cable.

Fluid force

Finally, the fluid force is added and according to Lin, Xiang, & Yang (2016) is written as:

$$F_D = -\frac{1}{2}\rho_f A_f C'_{Dyn} \left|\frac{\partial w(x,t)}{\partial t}\right| \frac{\partial w(x,t)}{\partial t} - \pi r^2 \rho_f C_m \frac{\partial^2 w(x,t)}{\partial^2 t},$$

(2.8)

where A_f represents the area facing flow, the density of the fluid is denoted as ρ_w, the dynamic flow coefficient is represented as C'_{Dyn} and C_m represents the mass coefficient. Empirically the values for C'_{Dyn} and C_m are 0,7 and 1,0 in water according to Lin, Xiang, & Yang (2016).

The two equations of motion, the Euler-Bernoulli beam equation and the external forcing, together with the boundary conditions and the initial conditions fully describes the problem. In the next paragraph the solution method is elaborated.

2.4 The solution method

The Differential Equations (DE's) (2.1), (2.2) and (2.5) need to be solved. Due to the interaction forces Q_1 and Q_2 these three equations are coupled; as is shown in equation (2.3). This set of coupled differential equations therefore needs to be solved simultaneously to find the solution.

To solve the Euler-Bernoulli equation, the method of separating variables and Modal Expansion is used. This implies that the solution for $w(x,t)$ is assumed as follows:

$$w(x,t) = \sum_{n=1}^{N} \varphi_n(x) q_n(t),$$

(2.9)

where N represents the number of modes considered, φ_n denotes the spatial dependency and q_n the time dependency of the beam's deflection.

The collection of deflection modes is solely determined by the characteristic of the beam. Therefore, the spatial dependency term can be found by inserting (2.9) into the Euler-Bernoulli beam equation (2.5) and solving for the homogenous solution. Considering the boundary conditions leads to:

$$\varphi_n(x) = C_n * \sin\left(\frac{k\pi}{L}x\right).$$

(2.10)

Due to these boundary conditions, φ_n is of a simple form. Consequently, it has been chosen to add the forcing of the tethers to the right side of the Euler-Bernoulli Beam equation, instead of using interface conditions.

Substituting the obtained solution (2.10) into (2.5) and using orthogonality, a sum of 2nd order ODE's is formed, see equation (2.11) (for further explanation of this method I would like to refer to bachelor thesis of De Graaf (2018)).

$$\sum_{k=1}^{K} \frac{\partial^2 q_k(t)}{\partial t^2} + \omega_k^2 \, q_k(t) = \int_0^L \frac{2}{\rho A L} \big(g(x,t) + F_s + F_{drag}\big) \varphi_k(x) dx, \tag{2.11}$$

where K denotes the number of modes taken into consideration and is equal to N.

All is left are 2nd order ODE's, which can be truncated to the amount of modes that need to be considered. By choosing this method of Modal Expansion, finite element methods can be avoided.

The spatial integral on the righthand side of equation (2.11) can be solved easily for the forcing of the vehicle $g(x,t)$ and the forcing in the tethers F_s, because of the spatial dependent Dirac function. But due to the complexity of the drag force, the first term of the fluid force (2.8), without a Dirac function and its non-linearity, this integration is solved using the trapezoidal tool 'trapz' in MATLAB.

2.4.1 Reduction to a set of first order ODE's

The MATLAB's ODE solver that is used requires the ODE's to be of first order. Therefore, the equations of motion and the Euler-Bernoulli beam equation are written in the state-space form. Every 2nd order ODE will turn into a set of two first order ODE's. MATLAB's 'ode45' solves all these first order ODE's simultaneously. 'Ode45' choses its own timestep to ensure the relative and absolute error that are imposed.

3. Work method and validation of the numerical model

In this chapter the chosen numerical model is validated. This validation is done by testing the limit cases against known and verified solutions. To build the numerical model, a work method of increasing complexity is used.

3.1 Increasing complexity and testing against limit cases

The MATLAB model is built by increasing its complexity throughout this thesis. Every increase in complexity was tested in limit cases against Graff's (1975) known solution of a single constant load moving across a simply supported beam:

$$w_{graff}(x,t) = \frac{2P}{\rho AL}\sum_{n=1}^{\infty}\frac{\sin(\beta_n x)}{\omega_n(\beta_n^2 v^2 - \omega_n^2)}\left[\beta_n v\sin(\omega_n t) - \omega_n \sin(\beta_n v t)\right],$$

where $\omega_n = \sqrt{\frac{EI}{rho*A}}\left(\frac{n\pi}{L}\right)^2$, $\beta_n = \frac{n\pi}{L}$ and P represents the load.

(Graff, 1975)(3.1)

Firstly, a model is formulated where there are two constant loads moving across the beam, where the distance between the loads represents the wheelbase. In the limit case with the wheelbase set to 0.001, it represents a single load and can be tested against Graff. Secondly, the inertia of the vehicle with the springs and dashpots is introduced. This is the result from De Graaf's (2018) bachelor thesis. To test against Graff's equation, again the wheelbase had to be set to zero, and the stiffness of the springs and the dashpot coefficient c theoretically set to infinity. Numerical models do not accept infinity, so it can be chosen to impose large numbers. How large k should be chosen also depends on the parameters of the bridge. It must be chosen so that it satisfies the relative error. Physically this makes perfect sense since they both influence the magnitude of the forcing acting on the bridge.

Finally, the forcing from the tethers and the fluid force are introduced one-by-one. This is validated in the limit cases, equally as stated above. The spring constant in the tethers is set to 0.0001; the dynamic fluid coefficient and the mass coefficient are set to 0.001.

3.2 Validation of the model

In this part only the validation of the models with the tether forcing and the fluid forcing is shown. These models are built from the simpler models without these forces. Therefore, the simpler models show a better relative error and are not displayed. The models are only tested while the vehicle is on the bridge, the solution is trusted to be accurate for free vibration. The tolerance is adjusted in the ODE solver, so that it stays below 0.5%.

The velocity of the vehicle is set at $40\ m/s$ and the length of the tunnel at $100\ m$, further parameters used for the validation are the same as shown in chapter 4 for the tunnel, apart from the limit cases for the spring's and dampers, described in 3.1.

Firstly, the number of modes that are to be considered must be known. Therefore, the relative error between the different number of modes chosen in the model and solution of Graff with twenty modes is shown in Figure 4. As can be seen; 6 modes in the model should be enough to represent the simply supported beam.

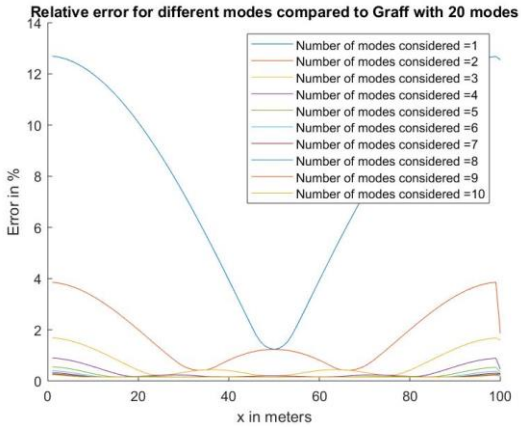

Figure 4 Relative error with different number of modes compared to Graff with 20 modes.

In Figure 5 the representation of the beam in the limit cases is shown for two models including ten modes, one considering the forcing from the tethers and the other also including the fluid interaction. The graphs almost perfectly overlap in the limit cases with Graff's known solution. This indicates that the model is a good representation of the situation.

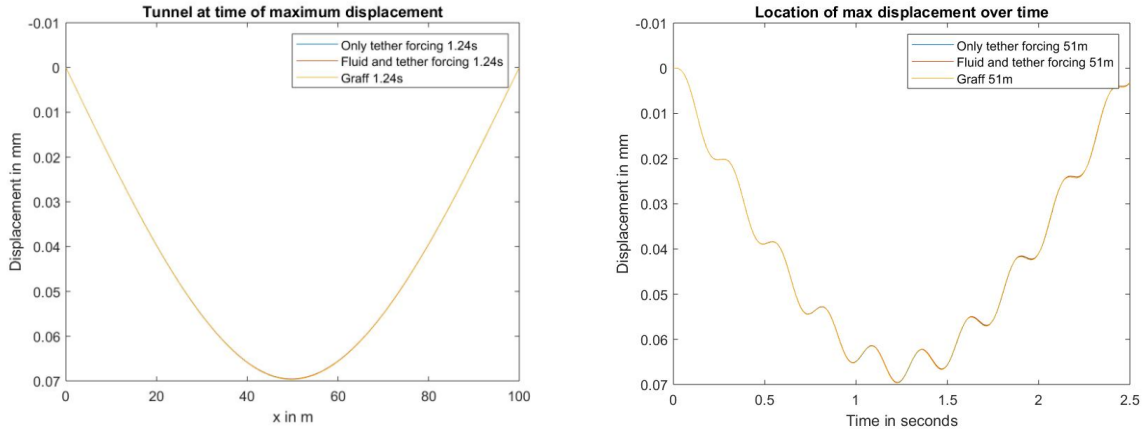

Figure 5 Left: the tunnel's displacement of the two models and Graff's solution at the time of maximum displacement. Right: he location of the max displacement against time.

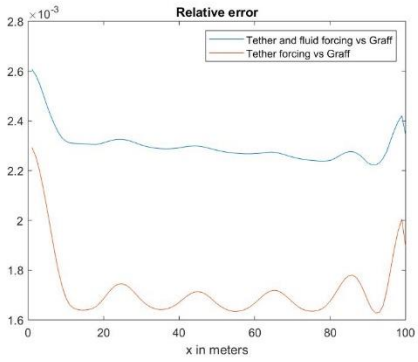

Figure 6 Relative error for both the tether and the fluid forcing, as well as only the tether forcing compared with Graff's solution.

Further, in Figure 6 the relative error for both models are shown. Both models meet the requirement of 0.5%. The MATLAB-code is found in Appendix A.

3.3 Limitations of the model

As can be seen in Figure 3 the horizontal and vertical motion of the tunnel are coupled. However, this model is limited to the response of the vehicle and tunnel in only the vertical direction.

The vehicle in this model is simplified to only two contact forces, but can be extended to incorporate more contact forces, to represent more than just one vehicle or a part of a train.

Another restriction is that the number of modes taken into account is limited to the user's choice. For the results to be accurate, enough modes need to be considered.

For the interaction with the fluid, the drag force and the added mass are considered. They both have their own coefficients which vary per situation or location of the tunnel. Also, the complete behavior of the fluid around the structure is therefore simplified. The effect of these simplifications might lead to slightly different results, which are partly explained in the next chapter.

Lin, Xiang, Yang and Chen (2016) showed that the horizontal flow does have an impact on the response in the vertical direction. Nevertheless, in this system the flow of the water is neglected.

4. Results for a simply supported beam and the SFT

In this chapter the models are used to analyze a simply supported bridge and the Submerged Floating Tunnel (SFT). The first part of this chapter only analyzes a simple supported beam, without tether forcing nor the force of the fluid. In paragraph 4.2 and 4.3 is the response of the SFT and the vehicle through a series of parametric studies investigated. In this chapter the word vehicle and train are used interchangeably and mean the same.

4.1 Utilizing the model for a simply supported beam

In this paragraph a simply supported bridge is analyzed. By adjusting certain parameters, it is possible to see if the inertia of the vehicle influences the ULS and under what circumstances it does so. The displacement is a good start to check for any ULS issues. The displacements of the two different models (with inertia and constant moving loads) are compared. Correspondingly, the displacement of a static point load at midspan is compared to the models. According to the classic forget-me-not, the displacement for a static point load is given by:

$$w = \frac{1}{48}\frac{(\mathrm{M} * \mathrm{g})\mathrm{L}^3}{EI}. \qquad (4.1)$$

Following the research of De Graaf (2018), the same parameters are used for the bridge and the train if not stated otherwise. These parameters are shown in Table 1.

Table 1 Bridge and vehicle parameters for a simply supported beam (De Graaf, 2018).

Bridge parameters			**Vehicle parameters**		
Density	2400	kg/m^3	Velocity	55.6	m/s
Cross-sectional Area	26.15	m^2	Mass	28950	kg
Length/span	105	m	Inertia	60312.5	kg.m^2
Bending stiffness EI	6.28 E12	Nm^2	Spring stiffness	8.8 E5	N/m^2
			Damping Coefficient	6.0 E4	N.s/m
			Wheelbase	12.6	m

4.1.1 Constant moving point loads versus loading by a vehicle with inertia

For the constant point loads the weight of the train is equally divided over the two loads. For a simply supported bridge, with regular parameters, the maximum displacement due to two constant loads or a vehicle with inertia hardly makes a difference. In Figure 7 this is clearly visible. When some parameters of the beam are altered to unrealistic values, some minor differences can be seen, where the double constant load shows a higher displacement then the vehicle with inertia. This coincides with the findings from Yang, Yau and Wu (2004).

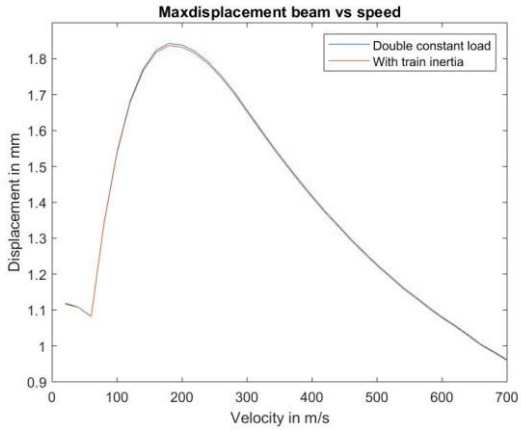

Figure 7 Maximum beam displacement at various velocities of a vehicle with inertia and a double constant load.

Critical velocities according to Graff

In Graff's (1975) solution for the simply supported beam an indeterminate solution could arise for certain velocities, he described them as critical velocities. These critical velocities could be written as follows:

$$V_n = \frac{\omega_n}{\beta_n} = \sqrt{\frac{EI}{\rho A}} * \frac{n\pi}{L}.$$

(Graff, 1975)(4.2).

Filling in the parameters of the simply supported beam for the first mode, leads to a velocity: $V_0 = 299.3\frac{m}{s}$. Indeed, as Graff (1975) noticed, at this critical velocity the maximum displacement occurs as the train is just leaving the bridge. However, as can be seen in Figure 7 it does not always represent the maximum displacement. For the current model a lower velocity leads to a maximum displacement.

4.1.2 Comparing to a single static point load

For some different parameters of the bending stiffness the comparison to a static load case is made. The results are shown in the Table 2.

Table 2 Displacements in mm for different load cases.

EI	Displacement in mm		
	Static-load at midspan	Moving double load	Moving loads with train inertia
$6.28*10^{10}$	684.9	321.8	322.3
$6.28*10^{11}$	10.9	18.4	18.4
$6.28*10^{12}$	1.1	1.1	1.1

In the above table it is seen that one should take be aware with dynamic loading cases. The displacements for a bending stiffness of $6.28*10^{11}$, with all other parameters unaltered, lead to

much higher values in the dynamic loading analysis. An increase of roughly 80% in this case, which is outside the maximum safety factor of 1.67 for dynamic loading for well-maintained train tracks (Nederlands Normalisatie-instituut, 2015).

4.2 SFT analysis

In this part the submerged floating tunnel is analyzed. For the dimensions of the tunnel the research of Davide La Zara (2019) is used. If not mentioned otherwise the parameters used are shown in Table 3. Using the parameters in Table 3 is referred to as the base case.

Table 3 Input parameters for the SFT

Tunnel parameters			**Fluid parameters**		
Density	2615	kg/m^3	Density	1000	kg/m^3
Cross-sectional Area	65.78	m^2	Area facing flow	18	m^2/m
Length/span	1000	m	Dynamic flow coefficient	0.7	-
Bending stiffness EI	1.05 E14	Nm^2	Mass coefficient	1.0	-
Tethers			**Vehicle parameters**		
Spacing	50	M	Velocity	50	m/s
Spring-stiffness in z-direction	1.19 E8	N/m	Mass	34000	kg
			Inertia	60312.5	$kg.m^2$
			Spring stiffness	1.2 E6	N/m^2
			Damping Coeficient	3.44 E4	N.s/m
			Wheelbase	17.4	m

4.2.1 Modes considered

First, the number of modes that must be considered is investigated. It is important that the increase in modes used does not affect the deflection of the bridge. In Figure 8 the deflection of the bridge is shown for different amount of modes taken into consideration for the base case. It can be verified that more than 10 modes are only necessary for velocities higher than the resonant velocity. The number of modes may differ per case studied; these highly depend on the structure's parameters.

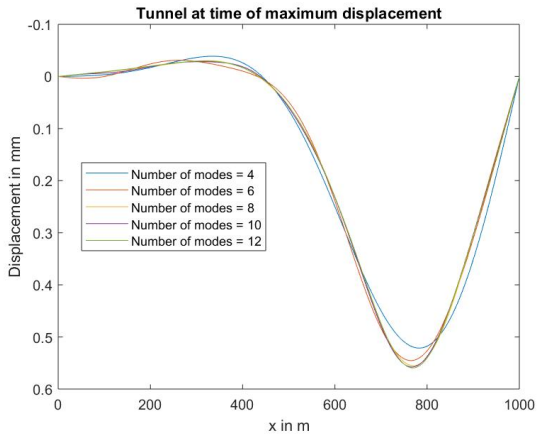

Figure 8 The effect of the number of modes considered on the deflection of the bridge.

4.2.2 Constant moving point loads versus loading by a vehicle with inertia.

The difference in maximum displacement of the tunnel between the vehicle with inertia or two moving point loads is negligible. The results are shown in Figure 9. The highest relative difference does not exceed 0.04%. These results are not surprising; for simply supported beams and for up to three spanned bridges this was also found by Yang, Yau, & Wu (2004).

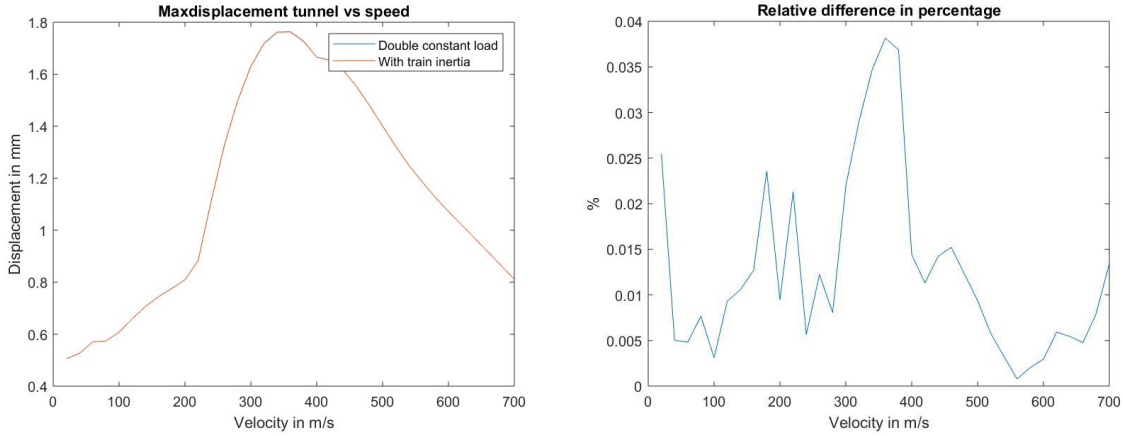

Figure 9 Left: the maximum tunnel displacement at various velocities of a vehicle with inertia and a double constant load. Right: the relative difference between the train cart with inertia and the double constant load.

The displacement increases significantly around the resonant velocity. At resonance velocity the displacement is more than three times higher than at low velocities.

The resonance is clearly visible for the blue line in Figure 10, where the length of the tunnel is increased to 2000 meters to see the amplification clearly. Although the resonant velocity may not seem relevant due to its large magnitude, it may be of interest in the future when vehicles could reach these velocities.

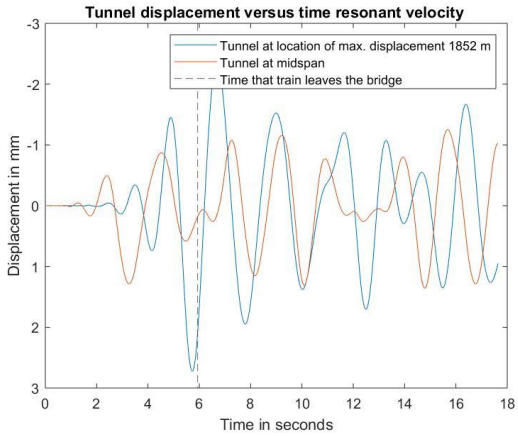

Figure 10 The displacement of the tunnel for resonant velocity (340m/s) at the location of its maximum displacement and at midspan.

Not only the maximum displacement is almost identical. The response of the bridge is also equal. The response is tested for the base case and can be found in Figure 11. For the figure on the left both midspan and the location of its maximum displacement perfectly overlap. It can be verified that for lower bending stiffness of the tunnel the relative difference is still negligible.

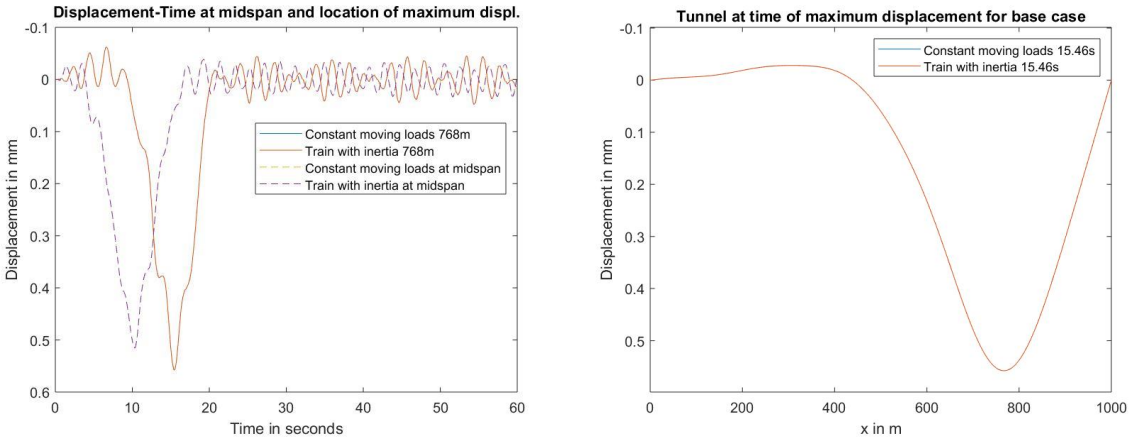

Figure 11 Left: the displacement-time diagram for the base case for both a vehicle with inertia and two moving point loads Rright: the position of the bridge at its maximum displacement.

4.2.3 Parametric studies

In this part parametric analyses are done for the mass coefficient of the fluid, the length of the tunnel and the spacing between the tethers. In all cases the influence of the train's velocity is investigated.

Mass coefficient of the fluid

The resonant velocities for the tunnel can be found in Figure 12 for different mass coefficients of the fluid, all other parameters are unaltered. The maximum displacement of the tunnel is set out against the speed.

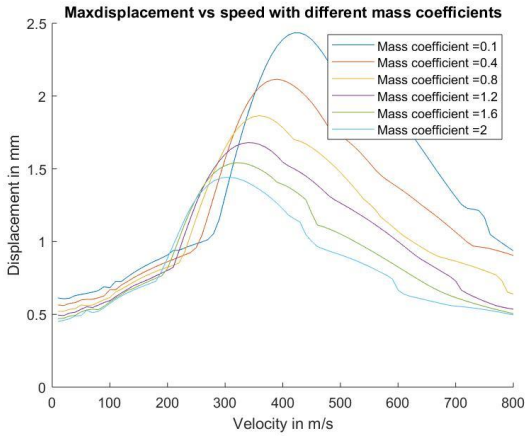

Figure 12 Maximum displacement of the tunnel against velocity for different mass coefficients.

The influence of damping, resembled by the mass coefficient of the fluid, clearly shifts the graph in Figure 12 to the left and lowers the resonance displacement. In the solution that Graff (1975) found for the critical velocity (Graff, 1975)(4.2). it can be seen that this velocity is inversely proportional to the square root of the mass of the beam. The shift of the graphs in Figure 12 Maximum displacement of the tunnel against velocity for different mass coefficients.to lower resonant velocities for increased mass of the SFT, might be caused by a similar relation that Graff found in 1975. For the exact solution of the resonant velocity more research is needed.

Length of the tunnel

The length of the tunnel has a significant effect on the displacement of the tunnel, which is shown in Figure 13. The amount of modes that are considered increases for longer tunnels.

The increase in tunnels length clearly shows an increase in maximum displacement, whereas the resonant velocity stays the same. Which means that the periodic forcing leading to this amplified displacement is not caused by the length of the tunnel. It explains that the passing of the tethers at a certain velocity is the main cause for resonance in Figure 13. For the tunnel of

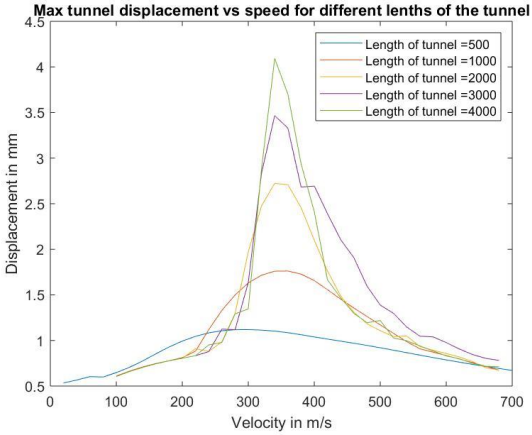

Figure 13 Maximum tunnel displacement at different velocities and different lengths of the tunnel.

500m it looks like the amplification did not have enough time to start resonating, and therefore does have a lower resonant velocity.

Nils Erik Anders Rønnquist (Chow, 2019) mentioned that, if the buoyancy is balanced correctly, the tunnel could be as long as the designer would like. However, the displacement of the tunnel, at resonant velocity, for the base case is already three times higher than for low velocities, and only increases for longer tunnels. Therefore, for static conditions Rønnquist may be right, but Figure 13 clearly shows that such statements should be treated with upmost care.

Tether spacing

The tether spacing shows to have an impact on the maximum displacement, as is displayed in Figure 14. The larger spacing between the cable supports allow for more possible displacement. Also, the resonant velocity is influenced by the spacing of the tethers. As Tariverdilo, Mirzapour, Shahmardani, Shabani and Gheyretmand (2011) already investigated the significant impact of the cable's stiffness, it can be concluded that combinations of these two parameters cause for different resonant velocities.

Also, it further explains that the passing of the tethers at a certain velocity leads to a periodic forcing engaging resonance. Again comparing to Graff's (1975) critical velocity ((Graff, 1975)(4.2) for a simply supported beam, he showed that this velocity is inversely proportional to the length of the beam. In the limit case when the tethers are infinitely stiff the tunnel represents a beam on multiple stiff supports. Although the closed form for a critical velocity of the vehicle is not found and the spacing between the tethers does not represent a simply supported beam, the critical velocity might be inversely proportional to the spacing between the tethers. This explains the shift of the graphs in Figure 14 to the left for larger spacing. Further investigation into the critical velocity is needed to verify this claim.

A dynamic loading analyses is nonetheless always advised for the design of the SFT, even without the full expression for the critical velocity.

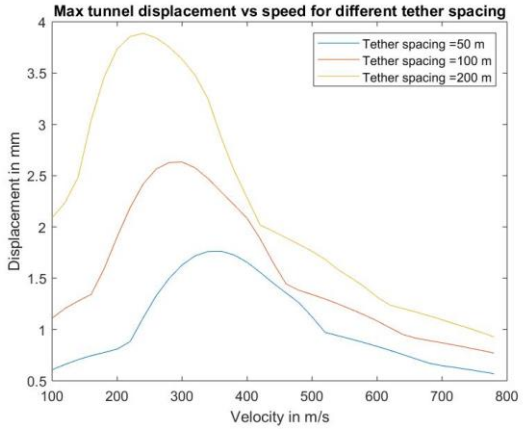

Figure 14 Influence of tether spacing on displacement and resonant velocity.

4.3 Vehicle analysis through parametric studies

According to Yang, Yau, & Wu (2004), the design of high-speed-railway bridges is usually determined by the serviceability conditions and not by the structural requirements. The limit for vertical acceleration for passenger comfort lies around $0.49\,\frac{m}{s^2}$. To calculate the acceleration the

Central Difference method is used on the velocity data generated by the 'ode45'-solver in MATLAB. For the train analysis the rail track is assumed to be perfectly smooth. The response of the vehicle is also investigated through a series of parametric studies and for different velocities.

Base case

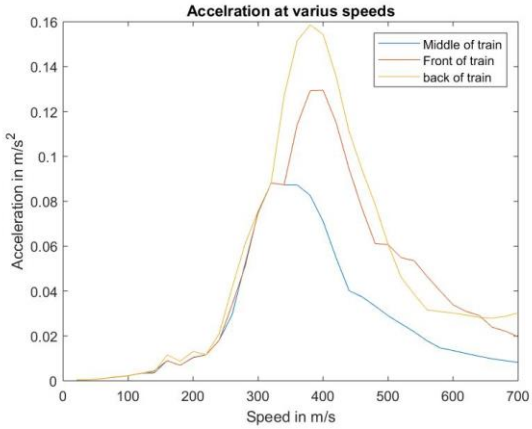

Figure 15 Maximum acceleration of the train at various speeds crossing the tunnel.

As can be seen in Figure 15, the vertical acceleration does not exceed the maximum allowance of $0.49\,\frac{m}{s^2}$, not even at resonant velocities.

Vehicle damping coefficient

Reducing the vehicle damping coefficients leads to, only at resonant velocities, a significant increase in acceleration, which are closer but do not exceed the maximum acceleration allowed. The maximum displacement slightly increases for lower damping coefficients. Although the exact movement of both bridge and vehicle differ in place and in time for every damping coefficient, the passenger comfort is always preserved.

Vehicle spring stiffness

The parametric study of the train's spring coefficient is performed for two damping coefficients. To have no influence from the damping coefficient it is set to 0.01 in one case. For the other case the damping coefficient is kept as mentioned in Table 3. The results of these studies are shown in Figure 16 and Figure 17.

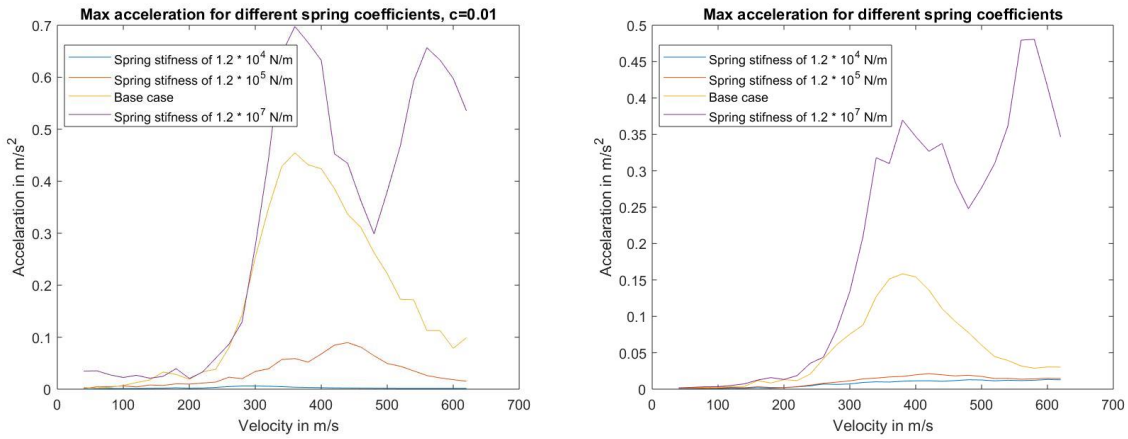

*Figure 16 Left: Maximum vertical acceleration for different spring stiffness. Left: neglecting the damping coefficient (c=0.01). Right: with 'normal' damping coefficient (c = 3.44*10⁴)*

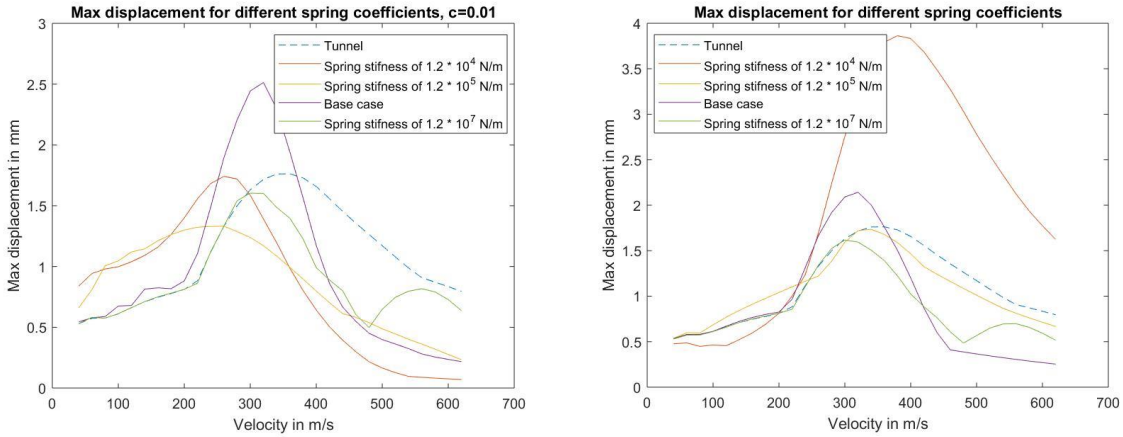

*Figure 17 Maximum displacement for different spring stiffness. Left: neglecting the damping coefficient (c=0.01). Right: with its normal damping coefficient (c = 3.44*10⁴)*

The effect of the lower spring stiffness at resonant velocities is interesting. It seems that lower spring stiffness could reduce the train's resonant displacement. Although this is depended on the damping coefficient and should be looked at per situation and combination. Lowering the stiffness of the vehicle's springs may also lead to other safety concerns, but these are not further investigated in this report.

Length of the tunnel

The maximum accelerations do increase, at resonant velocity, when the length of the tunnel is increase. For the current train parameters, the maximum acceleration does not seem to exceed the maximum of $0.49\,\frac{m}{s}$, as is shown in Figure 18. For tunnels longer than 6000 this does need to be verified.

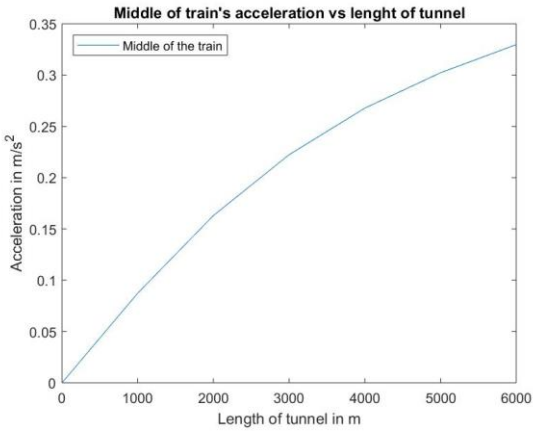

Figure 18 Maxximum acceleration of the middle of the train at resonant velocity for different tunnel lengths.

5. Conclusions & recommendations

5.1 Conclusions

This report investigated the interaction between a single vehicle, moving at constant velocity, and a submerged floating tunnel (SFT). More precisely, whether the vehicles inertia, the design of the SFT or the vehicles parameters had any effect on the Ultimate Limit State (ULS) of the tunnel or the Service Limit State (SLS) for passenger comfort. The following results were found:

1. The inertia of the vehicle has no significant effect on the displacements of the tunnel. For a vehicle with representative parameters; the relative difference in maximum displacement, compared to two constant moving loads, is less than 0.04% for any velocity. The displacement of the tunnel to moving loads could increase significantly and it is therefore recommended to include a dynamic study in the ULS calculations, instead of using a dynamic loading factor in the static analyses.
2. The length of the tunnel has a substantial effect on the maximum displacement of the tunnel and the vertical accelerations of the vehicle around the resonant velocity of 340 m/s. The length of the tunnel has no effect on the resonant velocity, which explains it is caused by the train passing the tethers at a certain velocity. The maximum tunnel displacement increased by a factor three for a tunnel of 1000 m compared to lower velocities. These amplifications only increased for longer tunnels. Therefore, a dynamic loading study is advised for the ULS investigations. Although the trains accelerations also increased, the maximum allowed acceleration of $0.49\,\frac{m}{s^2}$ for the SLS is never exceeded for any of the cases studied.
3. A larger spacing between the tethers leads to a lower resonant velocity. It is believed that the critical velocity of the tunnel might be inversely proportional to the spacing between the tethers. Further, for structural reasons, the spacing and the cable properties are dependent on each other. Tariverdilo, Mirzapour, Shahmardani, Shabani and Gheyretmand (2011) investigated the importance of the cable stifness. A dynamic study to the combination of the tether spacing, velocity of the vehicle and stifness of the tethers is therefore always recommended, to preserve the structural integrity of the tunnel.
4. An increase of the added mass coefficient of the fluid leads to a lower resonant velocity, which might be caused by some inverse relation between the mass and this velocity.
5. Changing the vehicle's damping coefficient or the spring stiffness causes for significant changes in displacements and accelerations of the vehicle. Nevertheless, the maximum allowed acceleration is only exceeded for a very stiff vehicle spring and neglecting the dashpots. With the studies performed there is no reason to believe that the interaction between the tunnel and the train lead to unacceptable accelerations.

5.2 Recommendations

This investigation was limited to only a single vehicle with two axles. To better represent the reality, it is suggested that more research will be done between the interaction of more vehicles or multiple train carts and the tunnel. Additionally, it is suggested to also investigate moving loads moving in opposite direction, on both the vehicle's and tunnel's response. Further, the vertical displacement is coupled to the horizontal displacement and it would be interesting to

analyze if the flow or current of the fluid influences the resonant velocities or displacements. At last, additional investigation into the resonant velocity of the vehicle could lead to a concrete expression, showing the relation between the critical velocity, the mass of the tunnel and the tether spacing.

References

Chow, D. (2019, February 15). *World's first 'floating tunnel' proposed in Norway*. Retrieved May 4, 2019, from Mach: https://www.nbcnews.com/mach/science/world-s-first-floating-tunnel-proposed-norway-ncna971581

De Graaf, A. (2018). *Theoretical model and application of a damped two degree of freedom spring-mass system, moving across a simply supported beam.* Delft: TU Delft.

Graff, K. F. (1975). *Wave Motion in Elastic Solids.* London: Oxford University Press & Ohio State University Press (n.p.).

La Zara, D. (2019). Torsion and Sprung Masses and Environmental - Damping Variation. Delft.

Lin, H., Xiang, Y., & Yang, Y. (2016, December 7). Coupled Vibration Analysis of CFRP Cable-tube System under Parametric Excitation in Submerged Floating Tunnel. *Procedia Engineering*(166), 45-52.

Lin, H., Xiang, Y., Yang, Y., & Chen, Z. (2018). Dynamic response analysis for submerged floating tunnel due to fluidvehicle-. *Ocean Engineering*(166), 290-301.

Nederlands Normalisatie-instituut. (2015, October). NEN-EN 1991-2+C1 (nl). *Eurocode 1: Actions on structures - Part 2:*. Delft, Netherlands: Nederlands Normalisatie-instituut.

Pilato, M. D., Perotti, F., & Fogazzi, P. (2008, January). 3D dynamic response of submerged floating tunnels under seismic and hydrodynamic excitation. *Engineering structures*(30), 268-281.

Remseth, S., Leira, B. J., Okstad, K. M., Mathisen, K. M., & Haukås, T. (1999, Augustus-September). Dynamic response and fluid/structure interaction of submerged floating tunnels. *Computers & Structures*(72), 659-685.

Spijkers, J., Vrouwenvelder, A., & Klaver, E. (2005). *Structural Dynamics CT 4140: Part 1 - Structural Vibrations.* Delft: Delft University of Technology: Faculty of Civil Engineering and Geosciences.

Tariverdilo, S., Mirzapour, J., Shahmardani, M., Shabani, R., & Gheyretmand, C. (2011, May). Vibration of submerged floating tunnels due to moving loads. *Applied Mathematical Modelling*(35), 5413–5425.

Xiang, Y., & Yang, Y. (2017, January 13). Spatial dynamic response of submerged floating tunnel under impact load. *Marine Structures, Elsevier*, 20-31.

Yang, Y. B., Yau, J. D., & Wu, Y. S. (2004). *Vehicle-Bridge Interaction Dynamics: With Applications to High-Speed Railways.* Singapore: World Scientific Publishing Co. Pte. Ltd.

Appendix A: MATLAB-Code

```
global rho A L EI M g v W k c J l kss Alpha Gamma F0 rhow r Aff Cdyn Cm


% Tunnel parameters
rho = 2614    ;       % kg/m^3    Density
A = 65.78     ;       % m^2       Cross-sectional area
L = 1000      ;       % m         Span
EI = 1.05 * 10^14;    % Nm^2      Bending stifness
g = 9.81 ;            % m/s^2     Gravitational force


%Tetthers
l = 50    ;           % m
kss = 1.19*10^8;     % N/m
Alpha = 45;
Gamma = 50;


% Drag
rhow = 1000         ; % kg/m^3    Density water
r = 9               ; % m         Radius
Aff = 2*r           ; % m^2 ??    How big should x be
Cdyn = 0.7          ; % Dynamic flow coefficient
Cm = 1             ; % Mass coefficent


% Train parameters
v = 800;            % m/s       Velocity
W = 17.6 ;            % m         Wheelbase                    SET THIS TO ZERO to
check with Graff
k = 1.2 *10^6;        % N/m       Springstifness
c = 3.44 *10^4 ;        % N*s/m     Damping
M = 34000;            % kg        Force
J = 60312.5;         % kg*m^2    Inertia


timestep = 0.01;
t = [0:timestep:L/v*3];
p = 1:1:10;
xstep = 1;
x = (0:xstep:L);


omega = zeros (1,length(p))';
bheta = zeros(1,length(p))';
for n = 1:length(p)
   omega(n) = sqrt(EI/(rho*A)*(n*pi/L)^4);
   bheta (n) = (n*pi/L);
end
```

```
% % Getting Graff's solution in the same dimensions as the model used
% wgraff = zeros(length(x),length(t));
% for pp = 1:length(p)
%     for xx = 1:length(x)
%         for tt = 1:length(t)
%             y = (2*M*g/(rho*A*L))*sin((bheta(pp))*
x(xx))/(omega(pp)*(bheta(pp)^2*v^2-omega(pp)^2)) *
(bheta(pp)*v*sin(omega(pp)*(t(tt)))-omega(pp)*sin(bheta(pp)*(v*t(tt))));
%             wgraff(xx,tt) = wgraff(xx,tt) + y;
%         end
%     end
% end




%%%%%%%%%%%%%%%%%% with drag and tethers
options1 = odeset('RelTol',1e-7,'AbsTol',ones((4+length(p)*2),1)*1e-7);


y0I = zeros((4+length(p)*2),1);
y0I(1) = M*g/(2*k);


% solving the ODE and putting all the q's in an array
    [t1,Y1] = ode45(@(t,y)withdrag(t, y,omega,bheta,p),t,y0I, options1);
    udrag = Y1(:,1);
    thetadrag = Y1(:,3);
    q_star = zeros(length(t),length(p));
    for pp = 1:length(p)
        q_star(:,pp) = Y1(:,(3+pp*2));
    end


% modally summing the small q's to get displacement wIdrag
wIdrag = zeros(length(x),length(t));
for xx = 1:length(x)
    w_starI = zeros(length(t),length(p));
    for pp = 1:length(p)
        w_starI(:,pp) = q_star(:,pp)*sin((bheta(pp))* x(xx));
    end
    wIdrag(xx,:) = sum(w_starI,2);
end


[maxdisplacementIdrag] = max (abs(wIdrag),[],"all");
```

```
[ixdrag,itdrag] = find(abs(wIdrag)==maxdisplacementIdrag);
LocationIdrag = ixdrag*xstep ;
TimeIdrag = itdrag*timestep ;


% %%%%%%%%%%%%%%%%%% without drag
% options1 = odeset('RelTol',1e-7,'AbsTol',ones((4+length(p)*2),1)*1e-7);
%
% y0I = zeros((4+length(p)*2),1);
% y0I(1) = M*g/(2*k);
%
% % solving the ODE and putting all the q's in an array
%     [t1,Y1] = ode45(@(t,y)withtraininertia(t, y,omega,bheta,p),t,y0I,
options1);
%     u = Y1(:,1);
%     theta = Y1(:,3);
%     q_star = zeros(length(t),length(p));
%     for pp = 1:length(p)
%         q_star(:,pp) = Y1(:,(3+pp*2));
%     end
% % end
%
% % modally summing the small q's to get displacement wI
% wI = zeros(length(x),length(t));
% for xx = 1:length(x)
%     w_starI = zeros(length(t),length(p));
%     for pp = 1:length(p)
%         w_starI(:,pp) = q_star(:,pp)*sin((bheta(pp))* x(xx));
%     end
%     wI(xx,:) = sum(w_starI,2);
% end
%
% [maxdisplacementI] = max (abs(wI),[],"all");
% [ix,it] = find(abs(wI)==maxdisplacementI);
% LocationI = ix*xstep ;
% TimeI = it*timestep ;
%
%
% Dif_Double_vs_Inertia = maxdisplacementIdrag-maxdisplacementI;
```

```
function [dy] = withdrag (t,y,omega,bheta,p)

global rho A L EI M g v W k c J l kss Alpha Gamma rhow r Aff Cdyn Cm

H1 = (heaviside(t-W/v) - heaviside (t-(L+W)/v));
H2 = (heaviside(t) - heaviside (t-(L)/v));

% Fdrag
xstep1 = 1;
x1 = 1:xstep1:L;
```

```
C1 = 0.5*rhow*Aff*xstep1*Cdyn;
C2 = pi*r^2*rhow*Cm;

Fd = zeros(length(x1),1);
for n = 1:length(bheta)
    for xx = 1:length(x1)
        Fd(xx) = (Fd(xx) - C1 * abs(sin(bheta(n).*(x1(xx)))*y(4+n*2))*
sin(bheta(n).*x1(xx)) *y(4+n*2));
    end
end

Fdd = zeros(length(p),1);
for pp = 1:length(p)
    for xx = 1:length(x1)
       Fd(xx) = Fd(xx)*sin(bheta(pp)*x1(xx));
    end
    Fdd(pp) = trapz(x1,Fd);
end



% Tethers
C = kss;
K = L/l-1;
Ft = zeros(K,1);

for kk = 1:K
   for n = 1:length(bheta)
       Ft(kk) = Ft(kk) - C * sin(bheta(n)*kk*l)*y(3+n*2);
   end
end


%%% Stating the sum of all the tethers per mode
Fss = zeros(length(p),1);
for pp = 1:length(p)
    for kk = 1:K
        Fss(pp) = Fss(pp) + Ft(kk)*sin(bheta(pp)*kk*l);
    end
end


%Basic Q1 and Q2 not depended on displacement
Q1 = (k*(y(1)+W/2*y(3)) + c*(y(2)+W/2*y(4)));
Q2 = (k*(y(1)-W/2*y(3)) + c*(y(2)-W/2*y(4)));

%Looping Q1 and Q2 to add the summation of the displacement
for n = 1:length(bheta)
    Q1 = Q1 - k*sin(bheta(n)*(v*t-W))*y(3+n*2)*H1 -
c*sin(bheta(n)*(v*t-W))*y(4+n*2)*H1;
    Q2 = Q2 - k*sin(bheta(n)*(v*t))*y(3+n*2)*H2 -
c*sin(bheta(n)*(v*t))*y(4+n*2)*H2;
end
```

```
dy = zeros(4+(length(p)*2),1);    % a column vector

dy(1) = y(2);
dy(2) = g - 1/M * Q1 - 1/M * Q2;
dy(3) = y(4);
dy(4) = -(W/(J*2))*Q1 + (W/(J*2))*Q2;

% looping the modes so that all the q's can be solved
for pp = 1:length(p)
    dy(3+pp*2) = y((4+pp*2));
    dy(4+pp*2) = -(omega(pp)^2) *y((3+pp*2)) + 2/((rho*A+C2)*L) *
(Fdd(pp) + Fss(pp) + (Q1) * sin(bheta(pp)*(v*t-W))*H1 + (Q2) *
sin(bheta(pp)*v*t)*H2);
end

end

function [dy] = withtraininertia (t,y,omega,bheta,p)

global rho A L EI M g v W k c J l kss Alpha Gamma

H1 = (heaviside(t-W/v) - heaviside (t-(L+W)/v));
H2 = (heaviside(t) - heaviside (t-(L)/v));

% Tethers
C = kss;
K = L/l-1;
Ft = zeros(K,1);

for kk = 1:K
   for n = 1:length(bheta)
       Ft(kk) = Ft(kk) - C * sin(bheta(n)*kk*l)*y(3+n*2);
   end
end


%%% Stating the sum of all the tethers
Fss = zeros(length(p),1);
for pp = 1:length(p)
    for kk = 1:K
        Fss(pp) = Fss(pp) + Ft(kk)*sin(bheta(pp)*kk*l);
    end
end


%Basic Q1 and Q2 not depended on displacement
Q1 = k*(y(1)+W/2*y(3)) + c*(y(2)+W/2*y(4));
Q2 = k*(y(1)-W/2*y(3)) + c*(y(2)-W/2*y(4));

%Looping Q1 and Q2 to add the summation of the displacement
for n = 1:length(bheta)
    Q1 = Q1 - k*sin(bheta(n)*(v*t-W))*y(3+n*2)*H1 -
c*sin(bheta(n)*(v*t-W))*y(4+n*2)*H1;
```

```
    Q2 = Q2 - k*sin(bheta(n)*(v*t))*y(3+n*2)*H2 -
c*sin(bheta(n)*(v*t))*y(4+n*2)*H2;
end

dy = zeros(4+(length(p)*2),1);    % a column vector

dy(1) = y(2);
dy(2) = g - 1/M * Q1 - 1/M * Q2;
dy(3) = y(4);
dy(4) = -(W/(J*2))*Q1 + (W/(J*2))*Q2;

% looping the modes so that all the q's can be solved
for pp = 1:length(p)
    dy(3+pp*2) = y((4+pp*2));
    dy(4+pp*2) = -(omega(pp)^2) *y((3+pp*2)) + 2/(rho*A*L) * (Fss(pp) +
(Q1) * sin(bheta(pp)*(v*t-W))*H1 + (Q2) * sin(bheta(pp)*v*t)*H2);
end

end
```

Appendix B: Report Kick-off meeting (30-4-2019)

First meeting with my second supervisor Andrei Faragua.
It is important to clearly state what is to be investigated, the main question was not specific enough and is therefore changed to:

> How does a submerged floating tunnel that is supported by cables, react in the vertical direction to the interaction with a vehicle moving at constant velocity? More specifically, I will investigate if inertia of the vehicle plays a significant role in the Ultimate Limit State of the tunnel, and the Service Limit State for passenger comfort.

It will be necessary to compare a model where just 2 constant loads move through the tunnel with a model where inertia has been considered.
For the model with 2 constant loads the book of Graff should be used for information. (page 169 and 170)
The parameters that should be used for the train should be similar to those used by the Msc. Students working on the submerged tunnel. Karel will send me the details of these students.
Be aware of the limitations in your model and make sure to state these in your report.
Also, it is wise to start the research with the spring supports placed periodically, because the design of the tunnel would be a lot easier as Andrei mentioned. If it turns out that this is really bad for the ULS or SLS then we might opt to change this.

Some further math has been discussed:
The ode's that will be investigated in this thesis should be solved with an ode solver in MATLAB, it is important that we try to avoid using Duhamel's integral. And make sure to set-up the equations so that we do not need to solve complicated integrations.
For the non-linearity of the drag-force we will focus on this a little later, and probably I would need some help from my supervisors.

The constant in $\varphi_k(x) = C_1 \sin\left(\frac{k\pi x}{L}\right)$ drops out when combined with $w(x,t) = \sum_{k=1}^{K} \varphi_k(x) q_k(t)$ because it will be solved for q_k. (time depended amplitude)